J. Am. Soc. Mass Spectrom. (2015) 26:1931–1937
DOI: 10.1007/s13361-015-1223-x

RESEARCH ARTICLE

Inkjet-Printed Gold Nanoparticle Surfaces for the Detection of Low Molecular Weight Biomolecules by Laser Desorption/Ionization Mass Spectrometry

Alyssa L. M. Marsico,[1] Brian Creran,[1] Bradley Duncan,[1] S. Gokhan Elci,[1] Ying Jiang,[1] Timothy B. Onasch,[2] Joda Wormhoudt,[2] Vincent M. Rotello,[1] Richard W. Vachet[1]

[1]Department of Chemistry, University of Massachusetts-Amherst, Amherst, MA 01003, USA
[2]Aerodyne Research, Inc., Billerica, MA, USA

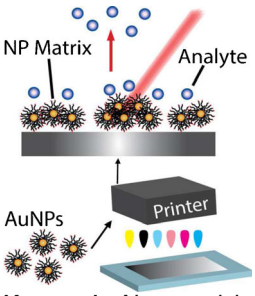

Abstract. Effective detection of low molecular weight compounds in matrix-assisted laser desorption/ionization (MALDI) mass spectrometry (MS) is often hindered by matrix interferences in the low *m/z* region of the mass spectrum. Here, we show that monolayer-protected gold nanoparticles (AuNPs) can serve as alternate matrices for the very sensitive detection of low molecular weight compounds such as amino acids. Amino acids can be detected at low fmol levels with minimal interferences by properly choosing the AuNP deposition method, density, size, and monolayer surface chemistry. By inkjet-printing AuNPs at various densities, we find that AuNP clusters are essential for obtaining the greatest sensitivity.

Keywords: Nanoparticles, Laser desorption/ionization, Inkjet-printing, Amino acids

Received: 19 March 2015/Revised: 22 June 2015/Accepted: 26 June 2015/Published Online: 23 July 2015

Introduction

Matrix assisted laser desorption/ionization mass spectrometry (MALDI-MS) is a powerful analytical tool that has been used to analyze many different biomolecules [1–5]. Using MALDI to ionize small molecules for mass spectrometric detection is beneficial because of the technique's inherent sensitivity and minimal sample consumption; however, analyzing small molecules by MALDI can be challenging because of matrix ion interferences in the low *m/z* region of the mass spectrum. Thus, finding alternate matrices that can facilitate ionization of low molecular weight compounds without producing interfering ions is of continued interest [2]. Nanomaterials have been investigated as alternatives to traditional organic matrices because they often have the proper optical properties to absorb UV laser light and facilitate ionization, while at the same time producing fewer interfering ions. Various types of nano-structured surfaces, including silicon and platinum [6–14], and different nanoparticles (NPs), including carbon-, silicon-, iron oxide-, titanium dioxide-, zinc oxide-based and noble metal NPs (gold, silver, and platinum) have been studied as alternate matrices [6, 15–25].

An attractive attribute of gold NPs (AuNPs), in particular, is the ease with which they can be functionalized using self-assembled monolayers. Such monolayer-protected NPs have tremendous potential as matrices because of the multidimensional control over their chemical and physical properties, while maintaining some of the inherent attributes that make them promising alternate matrices. AuNPs can be synthesized to have various monolayer ligands that offer different surface chemistries and variable core sizes. Russell and coworkers, for example, explored these attributes of AuNPs and found that surface chemistry and size have notable influences on ionization efficiencies of proteins and peptides [26, 27]. Cheng and coworkers synthesized AuNPs with monolayers of α-cyanohydroxycinnamic acid (CHCA), a common matrix used in MALDI, and found that this monolayer coating improved peptide ionization efficiencies compared with AuNPs with other monolayer coatings [28]. The CHCA monolayer, however, still gave rise to ion interferences in the low *m/z* region of the mass spectrum, mitigating to some extent the value of these particular NPs for the analyses of low molecular weight compounds.

Electronic supplementary material The online version of this article (doi:10.1007/s13361-015-1223-x) contains supplementary material, which is available to authorized users.

Correspondence to: Richard Vachet; *e-mail:* rwvachet@chem.umass.edu

Further studies of monolayer chemistry and size will allow for some additional level of control over the arrangement of these NPs on surfaces, which is important for optimizing how the laser energy is transferred to enable analyte ionization [29, 30]. Depending on the core size, monolayer ligand length, and monolayer chemistry, NPs can be assembled on surfaces to facilitate analyte ionization. Moreover, monolayer ligand chemistry could further be used to control which analytes interact with NP matrices, enabling selective ionization. In the work presented here, we describe the use of monolayer-protected AuNPs with varying surface chemistries as matrices for low molecular weight compounds. These AuNPs are deposited on surfaces to which analytes are then added, and thus this represents another example of surface assisted laser desorption/ionization (SALDI). We investigate how NP deposition method and NP monolayer chemistry influence the ionization efficiency of amino acids, which have been chosen as test analytes because they are biologically relevant small molecules. We find that inkjet-printing [25, 31–35] is a convenient and reproducible means of producing NP-coated surfaces that enable the very efficient ionization of these molecules.

Experimental

Chemicals

Arginine, histidine, glycine, glutamic acid, leucine, methionine, phenylalanine, serine, CHCA, glycerol, 1,2-hexanediol, and triethanolamine were purchased from Sigma Aldrich (St. Louis, MO, USA). Acetonitrile, nitric acid and hydrochloric acid were purchased from Fisher Scientific (Fairlawn, NJ, USA). MilliQ deionized water was obtained from a Millipore Simplicity 185 system (Billerica, MA, USA) and was used in all of the experiments. Aqua regia was prepared using nitric acid and hydrochloric acid, 3:1 (v:v). *Aqua regia is highly corrosive and must be handled with caution!*

Synthesis of AuNPs

The AuNPs used in these experiments (Figure 1) were prepared using previously published methods: TEGOH [36], TTMA [36, 37], and TEGCOOH [38]. In short, the Brust-Schiffrin two-phase synthesis method was used to synthesize pentanethiol-coated AuNPs with core diameters around 2 nm [39]. Subsequently, the Murray place-exchange method was used to functionalize TTMA and TEGCOOH. TEGOH was synthesized by the single-phase synthesis method described previously [40, 41]. After synthesis, each AuNP was dialyzed for 72 h against MilliQ water using a Spectra/Por Dialysis Membrane (molecular weight cutoff of 1000 Da) to separate the free ligands from the AuNPs. The resulting AuNPs were then characterized by transmission electron microscopy (TEM) to confirm the Au core size and LDI-MS to ensure proper monolayer attachment [42, 43].

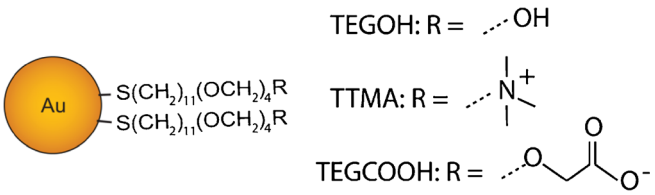

Figure 1. AuNPs with the indicated monolayer were used in the experiments

Analyte Sample Preparation

The amino acid solutions were prepared in deionized water. Once the AuNPs were deposited on the surface and dried, 1 µL of an amino acid solution was deposited on top of the AuNP surface. This solution was allowed to dry before MS analysis. For MALDI analyses, approximately 30 mg of CHCA was dissolved in 1 mL of a solution containing 70% acetonitrile and 30% water and then mixed in a 1:1 volume ratio with the amino acid solution of interest. For the LDI-MS analyses, 1 µL of an amino acid solution was deposited directly onto a stainless steel surface.

AuNP Surface Preparation

To prepare the pipette spotted samples, 1 µL of a solution of AuNPs in 100% water was spotted onto a MALDI target and allowed to dry. Then, 1 µL of the amino acid solution in water was spotted directly on top of the AuNP spot and allowed to dry prior to LDI analysis. The inkjet-printed AuNP surfaces were prepared using an Epson Artisan 50 inkjet printer (Long Beach, CA, USA). To prepare the AuNP solution for printing, the AuNPs were added to a printing solution, which consisted of 69% water, 20% glycerol, 10% 1,2-hexanediol, and 1% triethanolamine. This solvent composition provides the proper viscosity to ensure reproducible printing. The final solution of 2 nm TEGOH AuNPs was at a concentration of 4 µM, the 4 nm TEGOH at 400 nM, the 6 nm TEGOH at 148.5 nM and the 8 nm TEGOH at 62.5 nM to keep the amount of gold consistent. The 13 nm citrate AuNP solution was at a final concentration of 4 µM. The resulting AuNP solution was then added to an empty black inkjet printer cartridge, and a metal slide was placed on the CD printing tray. The NPs were printed in grayscale, going from 100% black (RGB = 0) for the high concentration end to white, or 0% black (RGB = 255), at the low concentration end using the printer software. The slides were covered with a petri dish top to prevent contamination and allowed to dry. Given the low volume droplets (~pL) deposited by the printer, the printed slides were microscopically dry within minutes; however, the slides were allowed to dry for 24 h before spotting 1 µL of analyte onto the surface.

Transmission Electron Microscopy

The TEM analyses were done with a JEOL 100S transmission electron microscope. The measurements were done at 200.0 kV and at a magnification of 50,000× or 20,000×. AuNP in printing solutions were printed on copper grids at a specific RGB value and allowed to dry for 24 h before analysis. When

analyzing these TEM images, amorphous collections of three or more AuNPs were considered a cluster for the purpose of relating ionization efficiency with cluster formation.

ICP-MS Analysis

Inductively coupled plasma (ICP) MS experiments were done on a Perkin Elmer NEXION 300 X ICP mass spectrometer (Waltham, MA, USA). The operation rf power was 1.6 kW, and the nebulizer gas flow rate was within a range of 0.9–1 L/min. The plasma gas flow rate and auxiliary gas flow rate were 16.5 L/min and 1.4 L/min, respectively. The analog stage voltage and pulse stage for the detector were –1600 V and 950 V, respectively. The deflector voltage was set to –12 V, and 50 ms was selected for the dwell time during the operation of the ICP-MS. To determine the AuNP amounts in a given printed area, slides were rinsed with 1 mL of an aqua regia solution and diluted to a final volume of 10 mL with MilliQ water. The slides were incubated in the same aqua regia solution for 1 h to dissolve the gold on the slide surface. The slides were then removed, and the remaining solution was analyzed by ICP-MS. Calibration standard solutions of 0, 0.2, 0.5, 1.0, 2.0, 5.0, 10.0, and 20.0 ppb of gold were used to quantify the amount of gold on the slides.

SALDI, MALDI and LDI-MS Analysis

We conducted three basic studies with different experimental substrates for comparison purposes: SALDI, MALDI, and LDI. SALDI experiments involved depositing AuNPs onto a stainless steel target and then depositing analyte on top. MALDI experiments were performed according to the typical protocol that involves co-crystallization of a matrix with the analyte. LDI experiments were conducted by depositing analyte onto a stainless steel surface without the addition of AuNPs or matrix. The effect of laser energy, as reported by the instrument software, on the resulting ion signal was investigated to find the optimum laser energy for SALDI, MALDI, and LDI. An example data set can be seen in Figure S1 in the Supporting Information. A laser energy of 70% was used for the SALDI and MALDI experiments, whereas a laser energy of 85% was used for the LDI experiments. The optimum laser energy of 70% was independent of the AuNP sizes used in the SALDI experiments.

SALDI, MALDI, and LDI MS experiments were done in positive mode on a reflectron-type time-of-flight (TOF) Bruker Autoflex III Smartbeam mass spectrometer that is equipped with a 355 nm Nd:YAG laser (Billerica, MA, USA). About 50 laser shots were fired at a frequency of 100 Hz to collect one spectrum with a reflectron voltage of 20.92 kV and an ion source voltage of 18.95 kV. The samples were prepared on stainless steel targets. In some cases, MS imaging was done on the samples using a raster width of 100 µm. After the imaging analyses, specific *m/z* values could be selected to generate images that simplified identification of optimal conditions.

Results and Discussion

Nanoparticle Deposition

Two different methods of depositing the AuNPs on surfaces were investigated. First, pipette spotting of the AuNPs with subsequent analyte addition on top was explored. This deposition method is simple and facilitates ionization of added amino acids. As an example, when 1 µL of a 100 nM solution of 2 nm AuNPs coated with TEGOH (see Figure 1) are spotted onto a target surface and 100 fmol of arginine is then added, peaks corresponding to protonated arginine (*m/z* 175) and sodiated arginine (*m/z* 197) are observed during SALDI-MS analysis (Figure 2). Analyte ions that could be isobaric with Au^+, such as sodiated arginine, can still be resolved from this interference, as organic molecules often have positive mass defects while Au has a negative mass defect. Comparable experiments in which no AuNPs are added result in no arginine-related ions during LDI-MS analysis, indicating how the functionalized 2 nm AuNPs enhance the ionization of this amino acid. Unfortunately, simple spotting of these AuNPs with a pipette does not give reproducible ion signal (see Figure S2 in the Supporting Information). The irreproducibility is attributed to "hot spots" that are generated as a result of the "coffee-ring effect" that occurs when the AuNPs dry after deposition on the surface, leaving a surface of AuNPs that is not homogeneous. These hot spots enhance ion signals in some areas but not others, depending on where the AuNPs deposit after drying (Figure 3a).

As an alternative to pipette spotting, we investigated inkjet-printing as a means of depositing a more homogeneous layer of AuNPs. Inkjet-printing has been used by our group and others to deposit NPs on a surface [25, 31–35]. Upon printing 2 nm TEGOH AuNPs we find that the AuNPs are more homogenously distributed than pipette spotting (Figure 3), and as a result analyte ions can be detected by SALDI-MS anywhere on the printed surface. When printing AuNPs as a matrix,

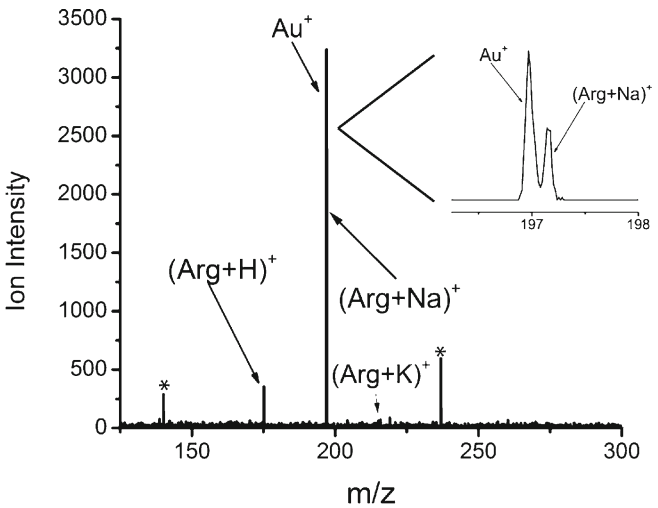

Figure 2. Detection of 100 fmol of arginine with the assistance of 2 nm TEGOH AuNPs; The asterisks (*) indicate peaks from an unknown contaminant seen when using the pipette spotting method. Inset: resolved Au+ and (Arg + Na)+ peaks

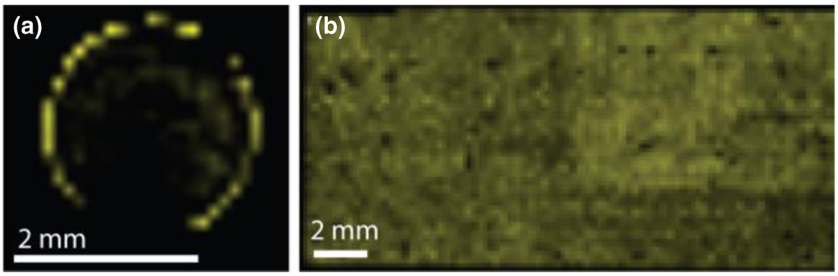

Figure 3. **(a)** Gold ion signal (*m/z* 197) obtained by LDI-MS when using pipette spotted AuNPs. **(b)** Gold ion signal obtained by LDI-MS on a surface inkjet-printed with AuNPs

a wide range of amino acids can be successfully detected, including arginine, histidine, cysteine, glycine, glutamic acid, leucine, methionine, phenylalanine, and serine (see Figure S3 in the Supporting information for example spectra). This method of AuNP deposition also lets us readily test how various NP surface densities influence analyte ion signal (see below).

AuNP Density and Physical Characteristics

Having established inkjet-printing as a better way to deposit AuNPs for SALDI-MS, we next considered how AuNP monolayer chemistry and AuNP core size influenced analyte ionization efficiency. To do this, we synthesized and printed NPs with positively charged (TTMA), negatively charged (TEGCOOH), and neutral (TEGOH) monolayer functional groups (Figure 1). For all the AuNPs studied, ion signals for the amino acids could be detected at much lower concentrations than are possible without the AuNPs (i.e., LDI-MS), but the NP monolayer identity noticeably influenced the result. AuNPs with the neutral TEGOH monolayer were found to provide the best signal. As an example, TEGOH could detect down to 50 fmol of arginine, while TEGCOOH AuNPs could barely detect 250 fmol of arginine (Figure S4 in the Supporting Information). The AuNPs with the TTMA monolayer performed better than the AuNPs with TEGCOOH, allowing amino acids to be detected as low as 50 fmol, but there were more interfering ions present from the positively-charged TTMA monolayer than the TEGOH monolayer because of the ease with which the TTMA monolayer is ionized relative to the TEGOH monolayer [40, 42]. The effect of AuNP core size on ionization enhancement was also considered. Core sizes of 2, 4, 6, and 8 nm with TEGOH monolayers were investigated. We also studied 13 nm AuNPs that were stabilized with citrate; it is difficult to synthesize and stabilize 13 nm AuNPs with the same monolayers shown in Figure 1.

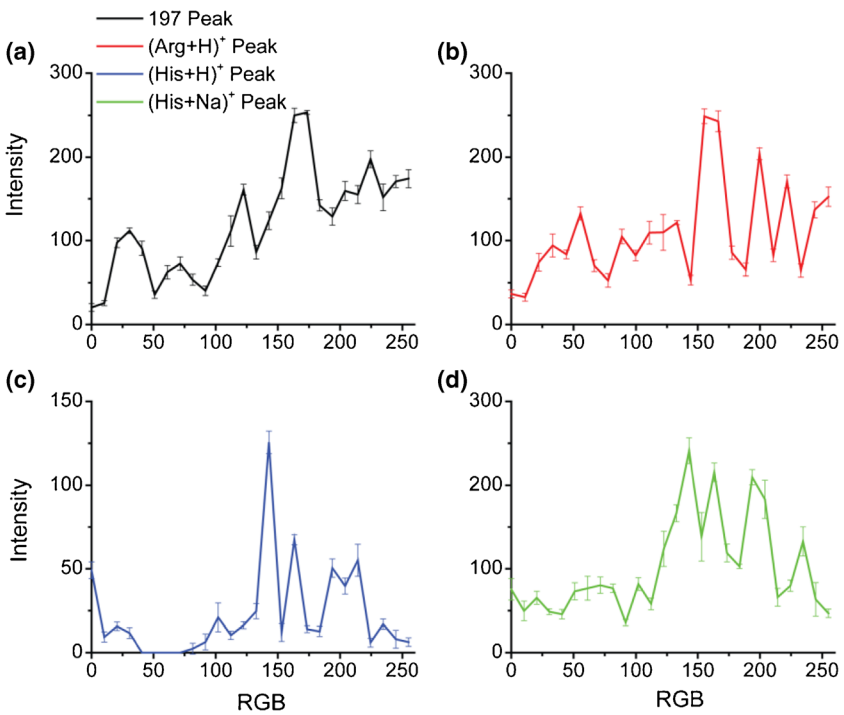

Figure 4. Intensity of signal from 250 pmol of spotted arginine and histidine across a RGB gradient of printed 2 nm TEGOH. **(a)** Signal from the *m/z* 197 peak, which arises from both the Au+ ion and the sodiated arginine ion. **(b)** Ion signal from protonated arginine. **(c)** ion signal from the protonated histidine peak. **(d)** ion signal from sodiated histidine

Table 1. Summary of the Characterization Results from the Surfaces Inkjet-Printed with 2 nm TEGOH AuNPs

Area of slide	ICP results (ng Au/cm^2)[a]	Average number of clusters per μm^2 [b]	Average NPs/cluster[c]	Average diameter of clusters (nm)[d]
High end of gradient (RGB = 0–20)	400–500	20 ± 10	4.4 ± 0.8	20 ± 3
Optimal region of gradient (RGB = 160–170)	2–5	38 ± 9	7 ± 4	30 ± 10
Low end of gradient (RGB = 245–255)	0–1	0	N/A	N/A

[a] Results were obtained by printing specific RGB values on glass slides and determining the printed gold by ICP-MS as described in the Experimental section. The resulting gold amounts were then converted to ng Au/cm^2 using the area assayed by ICP-MS
[b] These values were obtained by counting the number of clusters of AuNPs in a TEM sample area of approximately 0.25 μm^2
[c] These values were calculated by counting the number of AuNPs in each cluster
[d] These values were obtained from the diameter of each NP cluster

Analyte detection efficiency was explored for the different sized AuNPs by inkjet-printing different NP concentrations to find optimum NP densities on the printed surfaces. This was accomplished in a more high-throughput manner by printing AuNP gradients that went from high density to low density using different RGB values from the printer software, as described in the experimental section. After printing the NP gradients, rows of amino acid solutions at different concentrations were spotted onto the resulting surface and analyzed using MS imaging and ImageJ (Figure 4 and Figure S5 in the Supporting Information). With this approach, the optimal AuNP densities could be readily determined. As an example, the data in Figure 4 demonstrate that for 2 nm TEGOH AuNPs there is an optimum NP density corresponding to RGB values around 160–170 that enhances the analyte ion signals to the greatest extent. This RGB range corresponds to a density of NPs of around 2–5 ng Au/cm^2 (Table 1), which was determined using ICP-MS. Each of the different-sized NPs was printed in this same way. The optimal RGB values for the other NP sizes were 225–235 for the 4 nm AuNPs, 115–125 for the 6 nm AuNPs, 85–95 for the 8 nm AuNPs, and 230–240 for the 13 nm AuNPs. Each of these different core sizes enhanced the ion signal for amino acids compared with LDI-MS without AuNPs, but the 2 nm core materials routinely gave better signal, enabling 25 fmol of analyte to be detected in many cases.

Surface Characterization

Because the 2 nm TEGOH AuNPs reproducibly gave the best spectra and sensitivity, we further characterized the surfaces that were created upon inkjet-printing these AuNPs to understand how the NPs assembled on these surfaces. ICP-MS and TEM were used to determine how many AuNPs were present at specific RGB values and how the NPs were arranged on the surface. Three representative regions of the printed NPs were chosen for characterization: (1) the high end of the gradient, where the gold signal is the highest and some analyte signal is observed; (2) the optimal region where analyte signal is most enhanced; and (3) the low end of the gradient where some analyte signal is seen but no gold signal is observed. The results for these three regions are summarized in Table 1 and Figure 5. The ICP-MS results reveal that the gold surface densities are very different in each region, with the optimal region showing relatively low AuNP densities (i.e., 2–5 ng/cm^2). Interestingly, the TEM images show that the AuNPs are clustered together to a greater extent in the optimal region (Figure 5b), indicating that AuNP clusters are essential for efficient ionization. The high end of the AuNP gradient shows a homogenous distribution of individual and clustered AuNPs, but the average cluster size and cluster density are less than in the optimal region, which may explain why ionization is slightly less efficient in this higher concentration region. Linear arrangements, or "strings," of AuNPs are also present in a greater number in

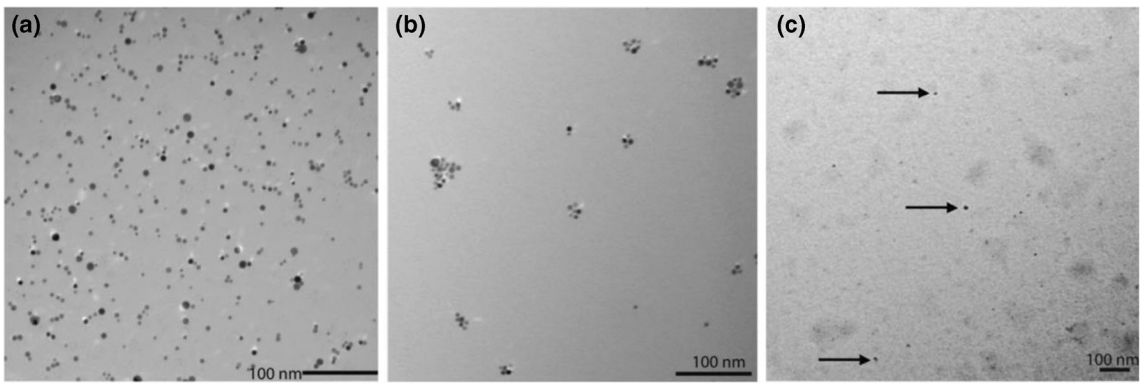

Figure 5. TEM images of **(a)** the high end of the inkjet-printed 2 nm TEGOH AuNP gradient, **(b)** the optimal region, **(c)** and the low end of the gradient where arrows point out AuNPs. The larger splotches in the low-end image are due to residual printing solution

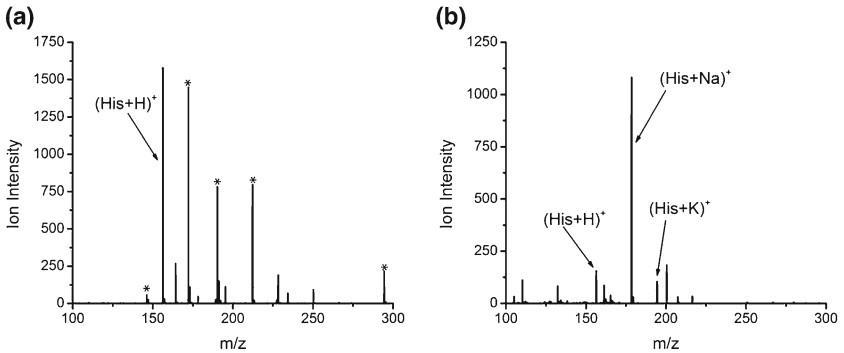

Figure 6. **(a)** MALDI mass spectrum of 500 fmol histidine with CHCA as the matrix; * marks matrix ion peaks. **(b)** SALDI mass spectrum of 500 fmol histidine after inkjet-printing 2 nm TEGOH AuNPs

the high end of the gradient, but these were not classified as clusters of AuNPs. Not surprisingly, the mass spectra from the high end of the gradient give higher Au^+ signals, and suppression from these higher Au^+ signals may explain the relatively lower analyte ion signals. Overall, the inkjet-printed gradient and the corresponding ICP-MS and TEM images demonstrate that the nature of the NP distributions on the surface influences ionization efficiency. It is likely that the larger NP clusters more effectively distribute the laser energy in a way that maximizes analyte desorption/ionization without extensive heating that might cause analyte degradation. The larger clusters may also spread out the energy such that fewer Au^+ ions are produced, thereby decreasing the abundance of this interference.

Comparison of SALDI to LDI and MALDI

When 2 nm TEGOH AuNPs are inkjet-printed at the optimal densities, amino acids such as arginine and histidine can be detected at levels as low as 25 fmol. This limit of detection is 2–3 orders of magnitude lower than previous approaches that have used NP-based matrices to detect amino acids [14, 44]. LDI-MS cannot detect amino acids anywhere near this level. MALDI-MS can detect amino acids at similar concentrations, but the spectra are more congested in the lower *m/z* region (Figure 6). This greater number of low *m/z* interferences in MALDI-MS is due to the presence of the organic matrix, which produces many different ion types. Under optimum conditions, the 2 nm TEGOH AuNPs produce Au^+ as the main interference, and its abundance is typically low.

Conclusions

Monolayer-protected AuNPs can assist the ionization of analytes in LDI-MS, acting in a manner similar to the organic matrix used in MALDI but with fewer low *m/z* interferences. If the proper NP surface chemistry and deposition method are chosen, AuNPs can assist ionization of amino acids with great efficiency, reproducibility, and with minimal interferences. From our experiments, we find that inkjet-printing, as opposed to simple pipette spotting, produces a homogeneous layer of AuNPs that enables reproducible analyte ionization. Interestingly, we find that NP cluster formation is required to obtain the lowest limits of detection, indicating that there is not only an optimal NP surface density but also that NP clustering plays an important role in analyte ionization mechanism. Future studies will investigate this underlying mechanism and will also explore AuNPs with monolayers that could be used to selectively extract analytes of interest from mixtures [45], while still allowing efficient ionization.

Acknowledgments

The authors acknowledge support for this work by the NSF (CMMI-1025020) and the SBIR grant NNX12CG18P from NASA.

References

1. Stults, J.T.: Matrix-assisted laser desorption/ionization mass spectrometry (MALDI-MS). Curr. Opin. Struct. Biol. **5**, 691–698 (1995)
2. Van Kampen, J.J.A., Burgers, P.C., de Groot, R., Gruters, R.A., Luider, T.M.: Biomedical application of MALDI mass spectrometry for small-molecule analysis. Mass Spectrom. Rev. **30**, 101–120 (2011)
3. Zhu, P., Bowden, P., Zhang, D., Marshall, J.G.: Mass spectrometry of peptides and proteins from human blood. Mass Spectrom. Rev. **30**, 685–732 (2011)
4. Kaufmann, R.: Matrix-assisted desorption ionization (MALDI) mass spectrometry: a novel analytical tool in molecular biology and biotechnology. J. Biotechnol. **41**, 155–175 (1995)
5. Trauger, S.A., Webb, W., Siuzdak, G.: Peptide and protein analysis with mass spectrometry. Spectroscopy **16**, 15–28 (2002)
6. Arakawa, R., Kawasaki, H.: Functionalized nanoparticles and nanostructred surfaces for surface-assisted laser desorption/ionization mass spectrometry. Anal. Sci. **26**, 1229–1240 (2010)
7. Wei, J., Buriak, J.M., Siuzdak, G.: Desorption-ionization mass spectrometry on porous silicon. Nature **399**, 243–246 (1999)
8. Go, E.P., Apon, J.V., Luo, G., Saghatelian, A., Daniels, R.H., Sahi, V., Dubrow, R., Cravatt, B.F., Vertes, A., Siuzdak, G.: Desorption/ionization on silicon nanowires. Anal. Chem. **77**, 1641–1646 (2005)
9. Chen, Y., Vertes, A.: Adjustable fragmentation in laser desorption/ionization from laser-induced silicon microcolumn arrays. Anal. Chem. **78**, 5835–5844 (2006)
10. Walker, B.N., Razunguzwa, T., Powell, M., Knochenmuss, R., Vertes, A.: Nanophotonic ion producion from silicon microcolumn arrays. Angew. Chem. Int. Ed. Engl. **48**, 1669–1672 (2009)
11. Walker, B.N., Stolee, J.A., Pickel, D.L., Retterer, S.T., Vertes, A.: Tailored silicon nanopost arrays for resonant nanophotonic ion production. J. Phys. Chem. C **114**, 4835–4840 (2010)

12. Finkel, N.H., Prevo, B.G., Velev, O.D., He, L.: Ordered silicon nanocavity arrays in surface-assisted desorption/ionization mass spectrometry. Anal. Chem. **77**, 1088–1095 (2005)
13. Kawasaki, H., Yonezawa, T., Watanabe, T., Arakawa, R.: Platinum nanoflowers for surface-assisted laser desorption/ionization mass spectrometry of biomolecules. J. Phys. Chem. C **111**, 16278–16283 (2007)
14. Nitta, S., Kawasaki, H., Suganuma, T., Shigeri, Y., Arakawa, R.: Desorption/ionization efficiency of common amino acids in surface-assisted laser desorption/ionization mass spectrometry (SALDI-MS) with nanostructured platinum. J. Phys. Chem. C **117**, 238–245 (2013)
15. Law, K.P., Larkin, J.R.: Recent advances in SALDI-MS techniques and their chemical and bioanalytical applications. Anal. Bioanal. Chem. **399**, 2597–2622 (2011)
16. Silina, Y.E., Volmer, D.A.: Nanostructured solid substrates for efficient laser desorption/ionozation mass spectrometry (LDI-MS) of low molecular weight compounds. Analyst **138**, 7053–7065 (2013)
17. Amini, N., Shariatgorji, M., Thorsén, G.: SALDI-MS signal enhancement using oxidized graphitized carbon black nanoparticles. J. Am. Soc. Mass Spectrom. **20**, 1207–1213 (2009)
18. Wen, X., Dagan, S., Wysocki, V.H.: Small-molecule analysis with silicon-nanoparticle-assisted laser desorption/ionization mass spectrometry. Anal. Chem. **79**, 434–444 (2007)
19. Kusano, M., Kawabata, S., Tamura, Y., Mizoguchi, D., Murouchi, M., Kawasaki, H., Arakawa, R., Tanaka, K.: Laser desorption/ionization mass spectrometry (LDI-MS) of lipids with iron oxide nanoparticle-coated targets. Mass Spectrom. **3**, A0026 (2014)
20. Chiang, C.-K., Chiang, N.-C., Lin, Z.-H., Lan, G.-Y., Lin, Y.-W., Chang, H.-T.: Nanomaterial-based surface-assisted laser desorption/ionization mass spectrometry of peptides and proteins. J. Am. Soc. Mass Spectrom. **21**, 1204–1207 (2010)
21. Lorkiewicz, P., Yappert, M.C.: Titania microparticles and nanoparticles as matrixes for in vitro and in situ analysis of small molecules by MALDI-MS. Anal. Chem. **81**, 6596–6603 (2009)
22. Watanabe, T., Kawasaki, H., Yonezawa, T., Arakawa, R.: Surface-assisted laser desorption/ionization mass spectrometry (SALDI-MS) of low molecular weight organic compounds and synthetic polymers using zinc oxide (ZnO) nanoparticles. J. Mass Spectrom. **43**, 1063–1071 (2008)
23. Pilolli, R., Palmisano, F., Cioffi, N.: Gold nanomaterials as a new tool for bioanalytical applications of laser desorption ionization mass spectrometry. Anal. Bioanal. Chem. **402**, 601–623 (2012)
24. Yonezawa, T., Kawasaki, H., Tarui, A., Watanabe, T., Arakawa, R., Shimada, T., Mafuné, F.: Detailed investigation on the possibility of nanoparticles of various metal elements for surface-assisted laser desorption/ionization mass spectrometry. Anal. Sci. **25**, 339–346 (2009)
25. Creran, B., Yan, B., Moyano, D.F., Gilbert, M.M., Vachet, R.W., Rotello, V.M.: Laser desorption ionization mass spectrometric imaging of mass barcoded gold nanoparticles for security applications. Chem. Commun. **48**, 4543–4545 (2012)
26. McLean, J.A., Stumpo, K.A., Russell, D.H.: Size-Selected (2–10 nm) gold nanoparticles for matrix assisted laser desorption ionization of peptides. J. Am. Chem. Soc. **127**, 5304–5305 (2005)
27. Castellana, E.T., Russell, D.H.: Tailoring nanoparticle surface chemistry to enhance laser desorption ionization of peptides and proteins. Nano Lett. **7**, 3023–3025 (2007)
28. Duan, J., Linman, M.J., Chen, C.-Y., Cheng, Q.J.: CHCA-modified Au nanoparticles for laser desorption ionization mass spectrometric analysis of peptides. J. Am. Soc. Mass Spectrom. **20**, 1530–1539 (2009)
29. Tarui, A., Kawasaki, H., Taiko, T., Watanabe, T., Yonezawa, T., Arakawa, R.: Gold-nanoparticle-supported silicon plate with polymer micelles for surface-assisted laser desorption/ionization mass spectrometry of peptides. J. Nanosci. Nanotechnol. **9**, 159–164 (2009)
30. Stolee, J.A., Walker, B.N., Zorba, V., Russo, R.E., Vertes, A.: Laser-nanostructure interactions for ion production. Phys. Chem. Chem. Phys. **14**, 8453–8471 (2012)
31. Singh, M., Haverinen, H.M., Dhagat, P., Jabbour, G.E.: Inkjet printing-process and its applications. Adv. Mater. **22**, 673–685 (2010)
32. Calvert, P.: Inkjet printing for materials and devices. Chem. Mater. **13**, 3299–3305 (2001)
33. Ko, S.H., Pan, H., Grigoropoulos, C.P., Luscombe, C.K., Fréchet, J.M.J., Poulikakos, D.: All-inkjet-printed flexible electronics fabrication on a polymer substrate by low-temperature high-resolution selective laser sintering of metal nanoparticles. Nanotechnology **18**, 345202 (2007)
34. Jang, J., Ha, J., Cho, J.: Fabrication of water-dispersible polyaniline-poly(4-styrenesulfonate) nanoparticles for inkjet-printed chemical-sensor applications. Adv. Mater. **19**, 1772–1775 (2007)
35. Gamerith, S., Klug, A., Scheiber, H., Scherf, U., Moderegger, E., List, E.J.W.: Direct Ink-jet printing of Ag–Cu nanoparticle and Ag-precursor based electrodes for OFET Applications. Adv. Funct. Mater. **17**, 3111–3118 (2007)
36. Ghosh, P.S., Verma, A., Rotello, V.M.: Binding and templation of nanoparticle receptors to peptide alpha-helices through surface recognition. Chem. Commun. **47**, 2796–2798 (2007)
37. You, C.-C., Miranda, O.R., Gider, B., Ghosh, P.S., Kim, I.-B., Erdogan, B., Krovi, S.A., Bunz, U.H.F., Rotello, V.M.: Detection and identification of proteins using nanoparticle-fluorescent polymer 'chemical nose' sensors. Nat. Nanotechnol. **2**, 318–323 (2007)
38. Hong, R., Emrick, T., Rotello, V.M.: Monolayer-controlled substrate selectivity using noncovalent enzyme–nanoparticle conjugates. J. Am. Chem. Soc. **126**, 13572–13573 (2004)
39. Brust, M., Walker, M., Bethell, D., Schiffrin, D. J., Whyman, R.: Synthesis of thiol-derivatised gold nanoparticles in a two-phase liquid–liquid system. J. Chem. Soc., Chem. Commun. **7**, 801–802 (1994)
40. Zhu, Z.-J., Ghosh, P.S., Miranda, O.R., Vachet, R.W., Rotello, V.M.: Multiplexed screening of cellular uptake of gold nanoparticles using laser desorption/ionization mass spectrometry. J. Am. Chem. Soc. **130**, 14139–14143 (2008)
41. Kanaras, A.G., Kamounah, F.S., Schaumburg, K., Kiely, C.J., Brust, M.: Thioalkylated tetraethylene glycol: a new ligand for water soluble monolayer protected gold clusters. Chem. Commun. **20**, 2294–2295 (2002)
42. Yan, B., Zhu, Z., Miranda, O.R., Chompoosor, A., Rotello, V.M., Vachet, R.W.: Laser desorption/ionization mass spectrometry analysis of monolayer-protected gold nanoparticles. Anal. Bioanal. Chem. **396**, 1025–1035 (2010)
43. Zhu, Z.-J., Rotello, V.M., Vachet, R.W.: Engineered nanoparticle surfaces for improved mass spectrometric analyses. Analyst **134**, 2183–2188 (2009)
44. Pilolli, R., Ditaranto, N., Di Franco, C., Palmisano, F., Cioffi, N.: Thermally annealed gold nanoparticles for surface-assisted laser desorption ionisation-mass spectrometry of low molecular weight analytes. Anal. Bioanal. Chem. **404**, 1703–1711 (2012)
45. Vanderpuije, B.N.Y., Han, G., Rotello, V.M., Vachet, R.W.: Mixed monolayer-protected gold nanoclusters as selective peptide extraction agents for MALDI-MS analysis. Anal. Chem. **78**, 5491–5496 (2006)